Available online at www.sciencedirect.com
SCIENCE DIRECT
Journal of Organometallic Chemistry 691 (2006) 3519–3530
Journal of Organometallic Chemistry
www.elsevier.com/locate/jorganchem

Synthesis, structure, electrochemistry, photophysics and electroluminescence of 1,3,4-oxadiazole-based *ortho*-metalated iridium(III) complexes

Lianqing Chen [a], Chuluo Yang [a,*], Jingui Qin [a,c,*], Jia Gao [b], Han You [b], Dongge Ma [b,*]

[a] *Department of Chemistry, Hubei Key Lab on Organic and Polymeric Optoelectronic Materials, Wuhan University, Wuhan 430072, China*
[b] *State Key Laboratory of Polymer Chemistry and Physics, Changchun Institute of Applied Chemistry, Chinese Academy of Sciences, Changchun 130022, China*
[c] *State Key Laboratory of Organometallic Chemistry, Shanghai Institute of Organic Chemistry, Chinese Academy of Sciences, Shanghai 200032, China*

Received 26 February 2006; received in revised form 29 April 2006; accepted 2 May 2006
Available online 7 May 2006

Abstract

Four new iridium(III) complexes **1**–**4**, with 1,3,4-oxadiazole derivative as cyclometalated ligand for the first time, have been synthesized and structurally characterized by NMR, EA, MS and X-ray diffraction analysis (except **1**). The stronger ligand field strength of the dithiolate ancillary ligands results in higher oxidation potentials and lower HOMO energy levels of complexes than acetylacetone. The absorption spectra of these complexes display low-energy metal-to-ligand charge transfer transition ranging from 350 to 500 nm. Complexes with dithiolate ancillary ligand emit at maximum wavelengths of ca. 500 nm, blue shifting 17 and 11 nm with respect to their counterpart with acetylacetone ligand. The electrophosphorescent devices with **2**–**4** as phosphorescent dopant in emitting layer have been fabricated. All devices have a low turn-on voltage in the range of 4.5 and 4.9 V. A high-efficiency green emission with maximum luminous efficiency of 5.28 cd/A at current density of 1.37 mA/cm^2 and a maximum brightness of 2592 cd/m^2 at 15.2 V has been achieved in device using **2** as emitter.

Keywords: Iridium complexes; 1,3,4-Oxadiazole; Dithiolate ligands; Photophysics; Electroluminescence

1. Introduction

In two decades, the photophysics and photochemistry of the heavy metal complexes have been extensively studied because of their long-lived excited states and high luminescent efficiency applicable to photoreductants, oxygen sensors, emissive materials, etc. [1]. Recently, heavy metal complexes as efficient phosphors in organic light-emitting diodes (OLEDs) have attracted much attention because the strong spin–orbit coupling by heavy metal ions incorporated in the complexes results in efficient intersystem crossing from the singlet to triplet excited states, enabling them utilize both singlet and triplet excited states [2]. Especially, the iridium(III) complexes with cyclometalated ligands show intense phosphorescence at room temperature and behavior as very promising phosphor dyes in OLEDs [3].

Oxadiazole derivatives have recently received considerable attentions in electro-active and opto-active materials due to their high electron affinities, which make them good candidates for electron injection and transportation [4]. Polymers containing oxadiazole units in the side chain or the main chain have been widely used in electronic devices for improving their electron-transporting ability [5]. Small molecular oxadiazole derivatives, such as 2-(4-*tert*-butylphenyl)-5-biphenyl-1,3,4- oxadiazole (PBD), have also been commonly used as electron-transporting and hole-blocking materials in OLEDs [6]. However, the

* Corresponding authors. Tel./fax: +86 27 68756757 (C. Yang).
E-mail address: clyang@whu.edu.cn (C. Yang).

0022-328X/$ - see front matter © 2006 Elsevier B.V. All rights reserved.
doi:10.1016/j.jorganchem.2006.05.003

oxadiazole-based metal complexes are very scarce. To our knowledge, only one palladium complex using oxidiazole derivatives as cyclometalated ligands has been reported [7].

From the view of ancillary ligand, a lot of cyclometalated iridium complexes with many kinds of ancillary ligands have been synthesized [8]. In particular, Thompson et.al. have studied the influence of ancillary ligand on the excited-state properties of cyclometalated iridium complexes [9]. However, no dithiolate as ancillary ligand has been involved. In fact, metal complexes containing dithiolate ligands have been widely reported. Platinum, gold and iridium(I) complexes with dithiolate ligands often exhibit interesting luminescent properties [10].

Based on the above consideration, here we report the synthesis and characterization of four new iridium(III) complexes with 2,5-di-*p*-tolyl-1,3,4-oxadiazole as cyclometalated ligand. Among of them, one is *tris-ortho*-metalated complex, one uses acetylacetonate (acac) as ancillary ligands, the other two use monoanionic dithiolates, *O*,*O*′-diethyldithiophosphate (Et_2dtp) or*N*,*N*′-diethyldithiocarbamate (Et_2dtc), as ancillary ligands (Scheme 1). The electrochemical, photophysical and electroluminescent properties of these complexes will be studied.

2. Experimental

2.1. General information

^{1}H NMR, ^{1}H–^{1}H COSY and one-dimensional NOE spectra were recorded on Varian Mercury VX-300 MHz spectrometer. ^{1}H–^{13}C COSY, ^{13}C NMR and ^{31}P NMR were recorded on Varian Unity Inova-600 MHz spectrometer. Elemental analysis of carbon, hydrogen, and nitrogen was performed on a Carlorerba-1106 microanalyzer. Mass spectra (FAB-MS) was determined by VJ-ZAB-3F Mass Spectrometer. Cyclicvoltammetry (CV) were recorded on CHI voltammetric analyzer. Anhydrous CH_2Cl_2 and THF were used as the solvent under nitrogen atmosphere, respectively. Tetra (*n*-butyl)-ammonium hexafluorophosphate ($TBAPF_6$) (0.1 M) was used as supporting electrolyte. The conventional three-electrode configuration consists of platinum working electrode, a platinum wire auxiliary electrode and an Ag wire quasi-reference electrode. The redox potentials were calibrated versus a ferrocenium/ferrocene (Fc^+/Fc) redox couple used as an internal reference. UV–Vis absorption spectra were recorded on Schimadzu 160A UV–Vis recording spectrophotometer. PL spectra were performed on Perkin–Elmer LS 55 luminescence spectrophotometer.

All reactions and manipulations were carried out under argon atmosphere. All silica gel column chromatography was performed with use of silica gel (200–300 mesh). 2, 5-Di-*p*-tolyl-1,3,4-oxadiazole [11], potassium *O*,*O*′-diethyldithiophosphate (KEt_2dtp) [12] and sodium *N*,*N*′-diethyldithiocarbamate ($NaEt_2$dtc) [13] were prepared according to the literature respectively. All other chemicals were used as received unless otherwise stated.

2.2. Synthesis of dimer $(tox)_2Ir(\mu\text{-}Cl)_2Ir(tox)_2$

Iridium trichloride hydrate (0.352 g, 1.0 mmol), combined with 2.5 equivalents of 2,5-di-*p*-tolyl-1,3,4-oxadiazole (0.625 g, 2.5 mmol), were dissolved in a mixture of 2-

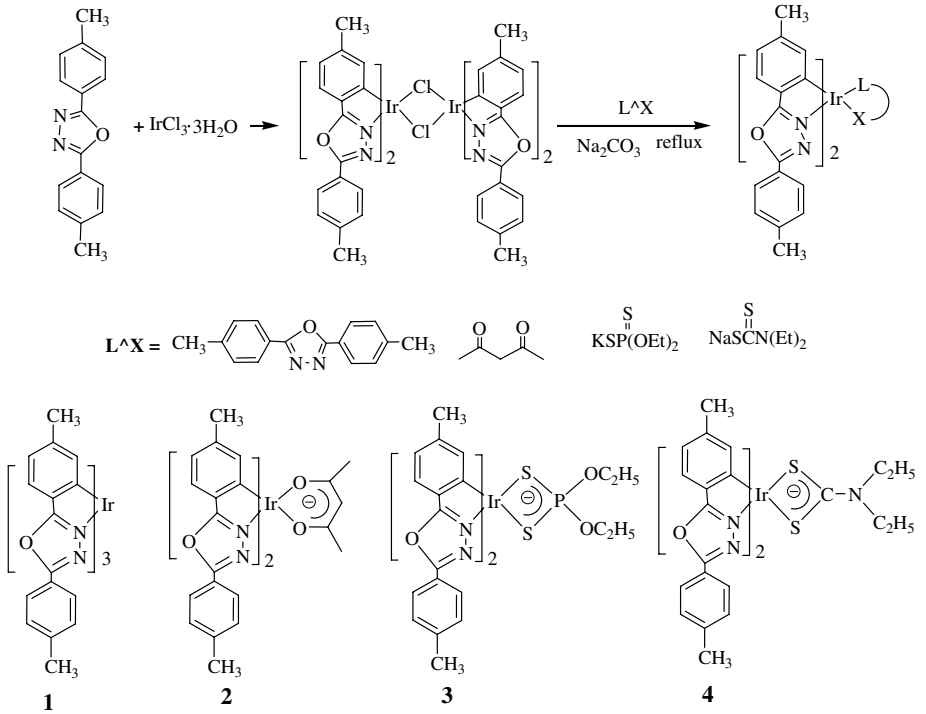

Scheme 1. Synthesis of $(tox)_2Ir$ (L^X) complexes.

ethoxyethanol (30 ml) and water (10 ml), and then refluxed for 24 h. The solution was cooled to room temperature, and the resulting yellow precipitate was collected on a glass filter frit. The crude product was washed with water, ethanol and hexane, and recrystallized from dichloromethane/hexane (1:1, v/v). Yield: 0.510 g (70%).

2.3. Synthesis of complexes

2.3.1. Complex *1*

Chloro-bridged dimer $(tox)_2Ir(\mu\text{-}Cl)_2Ir(tox)_2$ (120 mg, 0.0827 mmol), 2,5-di-*p*-tolyl-1,3,4-oxadiazole (62.5 mg, 0.25 mmol) and anhydrous sodium carbonate (Na_2CO_3)-(106 mg, 1.0 mmol) were dissolved in glycerol (10 ml). The solution was refluxed under argon gas atmosphere for 16 h. After completion of the reaction, small quantity aqueous hydrochloric acid (1 N) was added to the solution, resulting in precipitation of product. The precipitate was collected by filtration, washed with water, ethanol and hexane, and dried in vacuum. The crude product was purified by column chromatography on silica gel using CH_2Cl_2 as eluent. Yield (based on the dimer): 80%. Anal. Calc. for $C_{48}H_{39}O_3N_6Ir$: C, 61.13; H, 4.18; N, 8.94. Found: C, 60.98; H, 4.05; N, 8.63%. Ms (FAB): *m*/*e*, 941 (M^+).

2.3.2. Complex *2*

$(tox)_2Ir(\mu\text{-}Cl)_2Ir(tox)_2$ (120 mg, 0.0827 mmol), acetylacetone (25 mg, 0.25 mmol) and Na_2CO_3 (106 mg, 1.0 mmol) were dissolved in 2-ethoxyethanol (10 ml). The solution was refluxed under argon stream for 12 h. After cooling to room temperature, small quantity water was added. The yellow precipitate was collected by filtration, washed with water, ethanol and hexane, and dried in vacuum. The crude product was purified by by column chromatography on silica gel using CH_2Cl_2 as eluent. Yield (based on the dimer): 86%. Anal. Calc. for $C_{37}H_{33}O_4N_4Ir$: C, 56.26; H, 4.21; N, 7.09. Found: C, 56.01; H, 4.28; N, 6.94%. Ms (FAB): *m*/*e*, 790 (M^+).

2.3.3. Complexes *3* and *4*

The two complexes were synthesized according to the same method with **2** excepting using KEt_2dtp or $NaEt_2dtc$ to replace acetylacetone, respectively.

3. Yield (based on the dimer): 81%. ^{13}C NMR ($CDCl_3$, 600 MHz): 175.9, 163.3, 150.8, 143.0, 142.2, 134.4, 130.2, 126.8, 124.9, 123.2, 122.8, 120.9, 63.4, 22.2, 21.9, 16.5, 16.4. ^{31}P NMR ($CDCl_3$, 600 MHz): 106.5; Anal. Calc. for $C_{36}H_{36}O_4N_4S_2PIr$: C, 49.36; H, 4.14; N, 6.40. Found: C, 49.30; H, 4.01; N, 6.68%. Ms (FAB): *m*/*e*, 876 (M^+).

4. Yield (based on the dimer): 85%. ^{13}C NMR ($CDCl_3$, 600 MHz): 174.6, 162.1, 154.1, 141.3, 140.2, 133.6, 128.8, 125.9, 123.4, 121.8, 121.5, 120.2, 42.3, 30.9, 28.7, 28.3, 21.7, 20.9, 20.7, 13.1, 11.4. Anal. Calc. for $C_{37}H_{36}O_2N_5S_2Ir$: C, 52.96; H, 4.32; N, 8.55. Found: C, 52.57; H, 3.90; N, 8.89%. Ms (FAB): *m*/*e*, 839 (M^+).

2.4. Single crystal X-ray crystallography

Single crystals of complexes **2**–**4** were obtained by slow diffusion of diethylether to a dilute dichloromethane solution of these complexes at room temperature, respectively. Crystals suitable for X-ray diffraction studies were chosen from those yellow prisms and mounted in inert oil on a glass fiber for the cell determination, and data was collected using a Bruker SMART APEX2 CCD detector diffractometer using graphite-monochromatic Mo Kα radiation at 293 K. The unit cell parameters were determined from a least-squares fit of 100 accurately centred reflections ($4.14 < 2\theta < 55.00$; $3.24° < 2\theta < 54.96°$; $2.18° < 2\theta < 50.00°$). Heavy-atom method was employed to locate Ir atom and the remaining non-hydrogen atoms were located using cycles of difference Fourier maps and refined by full-matrix least-squares on F^2 using SHELXL-97 [14] suite of program. An empirical absorption correction using the program DIFABS [15] was applied. In the last refinement, all non-hydrogen atoms were described with anisotropic thermal parameters. Hydrogen atoms were introduced at calculated positions around aromatic rings. All figures were prepared using the program ORTEP3 for windows [16].

2.5. OLED fabrication and measurement

Organic layers were fabricated by high-vacuum thermal evaporation onto a pre-cleaned indium tin oxide (ITO). The glass substrates were sequentially cleaned by detergent, deionized, water, ethanol, acetone and chloroform in ultrasonic bath and heated in an ultra-infrared dry oven. In a vacuum chamber with a pressure of $<10^{-4}$ Pa, 40 nm of (4,4′-bis{*N*-(1-naphthyl-*N*-phenyl-amino)biphenyl})(NPB) as the hole transorting layer(HTL), 30 nm of Ir complexes doped 4,4′-biscarbazolybiphenyl (CBP) as the emitting layer, 10 nm of 2,9-dimethyl-4,7-diphenyl-1,10-phenanthroline (BCP) as a hole and exciton blacking layer, 30 nm of AlQ_3 as the electron *trans* porting layer (ETL), and a cathode composed of 1 nm of lithium fluoride and 100 nm of aluminum were sequentially deposited onto the substrate to construct the device. The *I*–*V*–*B* of EL devices was measured at ambient condition with a Keithey 2400 Source meter and a Keithey 2000 Source multimeter equipped with a calibrated silicon photodiode. The EL spectra were measured by JY SPEX CCD3000 spectrometer.

3. Results and discussion

3.1. Synthesis and characterization

Cyclometalated Ir(III) μ-chloro-bridged dimer, terakis (2,5-di-*p*-tolyl-1,3,4-oxadiazolato-C^2,*N*)(-dichloro)diiridium-$[(tox)_2Ir\text{-}(\mu\text{-}Cl)_2Ir(tox)_2]$, was synthesized by iridium trichloride hydrate with 2,5-di-*p*-tolyl-1,3,4-oxadiazole according to the similar method reported by Nonoyama

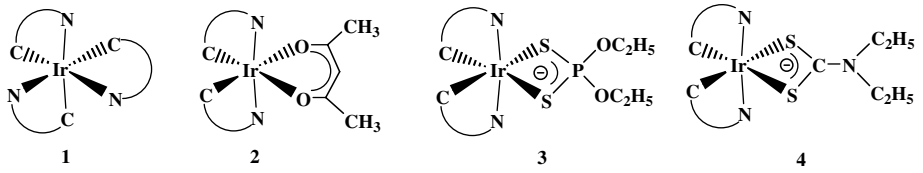

Fig. 1. The coordination geometries of the $(tox)_2Ir(L\hat{}X)$ complexes.

[17]. The *tris*-cyclometalated complex was synthesized by the reaction of the dimer with the oxadiazole ligand [18]. The other three iridium complexes were prepared by the dimer with corresponding ancillary ligands in 80–90% yield (Scheme 1). The chloride-bridged diiridium complex can be converted to mononuclear iridium complexes by replacing the two bridging chlorides with bidentate monoanionic L^X ligands. Elemental analysis of each of the four complexes is consistent with the expected formulation of their structures. The mass spectra give corresponding molecular ion peaks at 941 for **1**, 790 for **2**, 876 for **3**, and 839 for **4**, respectively. In addition, the mass spectra all show a peak at 691 for the four complexes, which arisen from the $Ir(tox)_2^+$ fragment.

3.2. NMR characterization

The solution structures of the complexes were established using ^1H NMR, and where applicable, ^{13}C NMR and 2D-COSY spectra. The ^1H NMR spectrum of *tris*-cyclometalated complex **1**, measured in $CDCl_3$ solution, displays five well-resolved signals (four doublets and one singlet) in the aromatic region between 7.8 and 6.3 ppm, suggesting a two-ring system with coupled groups of two and four spins corresponding to the unmetalated and metalated tolyl rings, respectively. The simplicity indicates that the three oxadiazole ligands surrounding the iridium atom are magnetically equivalent and the complex takes the facial structure (see Fig. 1). The metalated and unmetalated tolyl rings (labelled A and B, respectively, see Scheme 2) can be readily identified on the basis of the proton resonances. Protons on the metalated tolyl ring "A" experience larger shielding due to the electron-rich Ir–C moiety and thus appear at higher field than the corresponding protons on the unmetalated tolyl ring "B" [19]. The highest field resonance at 6.31 ppm is assigned to the proton (A_3) *ortho* to the metalated carbon atom. The protons of A_6 and B_6 (B_2) are deshielded because they are adjacent to electronegative nitrogen and oxygen

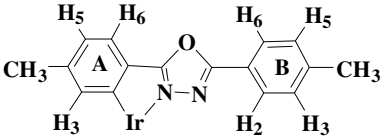

Scheme 2. Protons assignments of 2,5-di-*p*-tolyl-1,3,4-oxadiazole.

atoms of 1,3,4-oxadiazole ring, consequently, they appear at lower field than the protons of A_5 and B_5 (B_3). The ^1H NMR spectra data are summarized in Table 1. These assignments are similar to reported assignments in *ortho*-metalated phenylpyridine-based complexes [19,20].

Complexes **2**, **3**, **4** show similar patterns to complex **1** in the aromatic region (four doublets and one singlet), and the protons are assigned by using the same strategy. All ^1H NMR spectra assignments are compiled in Table 1. In these cases, the simplicities of the proton resonance indicate that the iridium center of **2**, **3**, **4** are coordinated by the two oxadiazole-based ligands with *cis*-C–C and *trans*-N,N chelate dispositions, which is different with the facial structure of complex **1**. It is noteworthy that in the aliphatic regions of **3** and **4**, two group multiplets, centered at 4.45, 4.15 ppm for **3** and 3.88, 3.48 ppm for **4**, respectively, were observed. The splitting patterns imply that the two protons at the same methylene of dithiolate ligands are magnetically inequivalent. Definitive assignments of the methylene protons come from 2D H–H COSY and NOE spectra. 2D H–H COSY spectra (Fig. 2) clearly show cross signals between the two group multiplets and also between the multiplets and methyl resonances. NOE spectra (Fig. 3) further confirm the assignment. When one proton of methylene was irradiated, a large NOE signal was observed and the splitting pattern became quartets from multiplets, assigning to another proton of the same methylene.

The ^{13}C NMR spectra of **3** and **4** all reveal 12 resonances in the aromatic region, corresponding to 12 types of carbon atoms of cyclometalated ligand. The simplicity

Table 1
^1H NMR spectrum data for the complexes

Complex	A				B			Ancillary ligand
	H_3	H_5	H_6	CH_3	H_3 (H_5)	H_2 (H_6)	CH_3	
1	6.31 s	6.66 d (7.5)	7.39 d (7.8)	2.04 s	6.96 d (7.5)	7.82 d (7.8)	2.23 s	
2	6.51 s	6.72 d (7.5)	7.48 d (8.1)	1.90 s	7.37 d (8.1)	8.12 d (8.1)	2.16 s	5.27 s (CH), 2.47 s (CH_3)
3	6.52 s	6.65 d (7.8)	7.40 d (7.8)	2.09 s	7.32 d (7.8)	8.02 d (7.5)	2.41 s	4.45 m (CH_2), 4.15 m (CH_2), 1.26 t (7.2, CH_3)
4	6.67 s	6.69 d (7.2)	7.48 d (7.2)	2.15 s	7.36 d (8.1)	8.14 d (7.5)	2.47 s	3.88 m (CH_2), 3.48 m (CH_2), 1.28 t (6.9, CH_3)

The values in parenthesis are coupling constant.

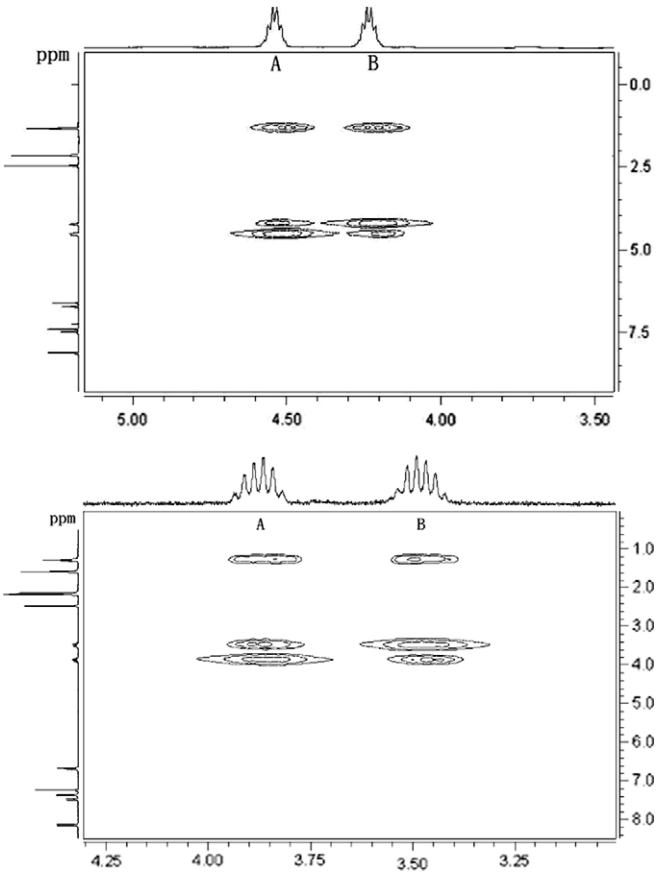

Fig. 2. Section of ^{1}H–^{1}H COSY Spectra of **3** (up) and **4** (down) in $CDCl_3$.

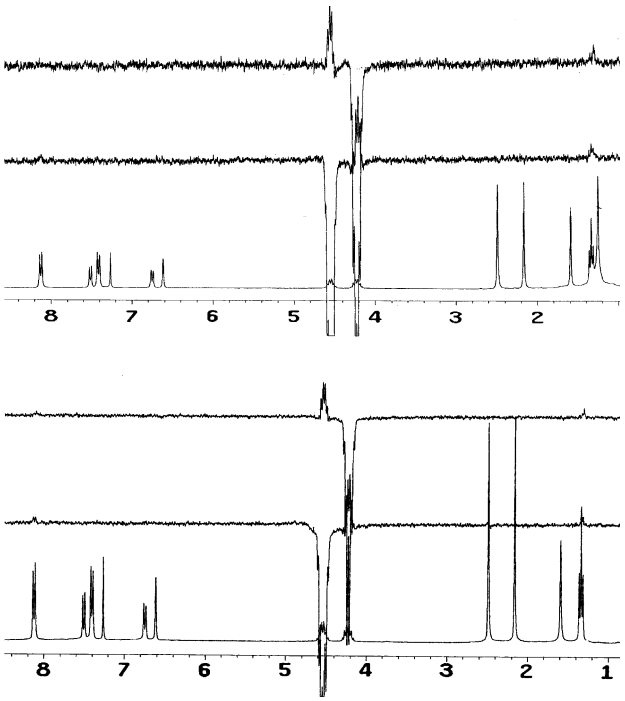

Fig. 3. One-dimensional NOE spectra of **3** (up) and **4** (down) in $CDCl_3$.

of the ^{13}C NMR spectra, like that of the ^{1}H NMR, supports the *cis*-C–C and *trans*-N–N chelate dispositions of the cyclometalated ligands with D_2 symmetry [2a,20]. The high-field resonances in the aliphatic region (four resonances for **3** and five resonances for **4**) can be easily assigned based on the 2D-H–C COSY. The 2D-H–C COSY (Fig. 4) shows the two group multiplets of ^{1}H NMR are related to the same carbon atom of methylene.

3.3. X-ray of crystallography

Single crystals of complex **2**, **3** and **4** suitable for X-ray diffraction studies were grown by slow diffusion of diethylether to a dilute dichloromethane solution of the complex. Molecular structures by ORTEP drawing are shown in Fig. 5. Crystallographic data are summarized in Table 2. Selected important bond distances and bond angles are given in Table 3.

All three complexes have distorted octahedral coordination geometry around iridium center by three chelating ligands with *cis*-C–C and *trans*-N–N dispositions. The N–Ir–N angles for these complexes are all almost 169°. The Ir–C_{aryl} bond lengths of complex **3** (2.032(4) and 2.029(4) Å) and complex **4** (2.050(16), 2.052(16),

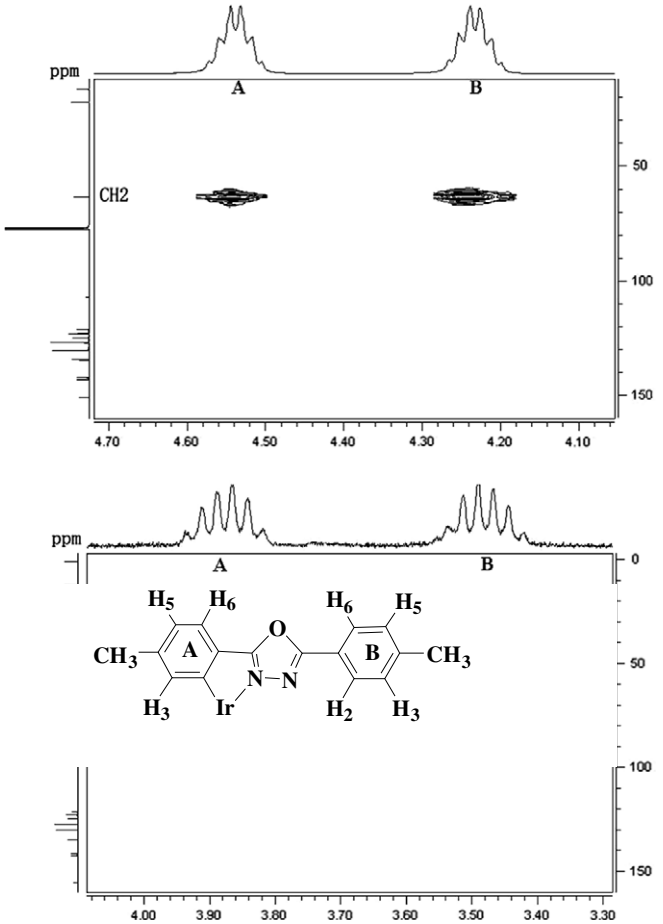

Fig. 4. Section of ^{13}C–^{1}H COSY spectra of **3** (up) and **4** (down) in $CDCl_3$.

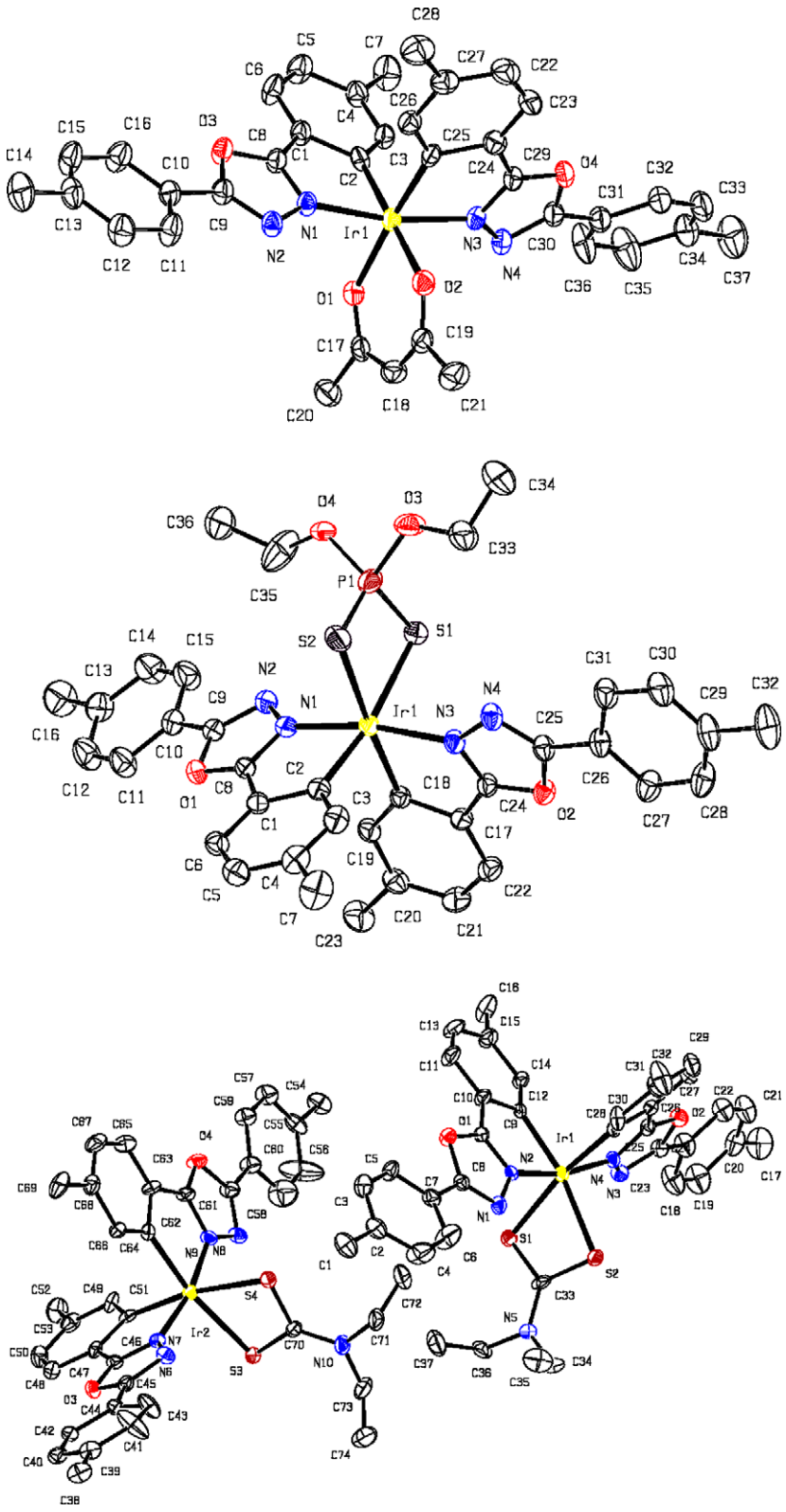

Fig. 5. ORTEP diagrams of **2** (top), **3** (middle) and **4** (bottom).The thermal ellipsoids are drawn at 30% probability level. The H atoms and solvent molecules are omitted for clarity.

2.048(17) and 2.052(19) Å) are longer than their counterpart complex **2** (1.986(5) and 1.978(5) Å). The average Ir–N bond distances of these complexes are not significantly varied. These values of Ir–C and Ir–N are similar to those reported in other mononuclear complexes with $(C^N)_2Ir$ fragment [2a,3c,9,18,21]. The similarity of bond lengths

between C 17–O1 (1.261(6) Å) and C19–O2 (1.280(6) Å) indicate that the −1 charge of the acetylacetone ligands is delocalized over both oxygen atoms. Likewise, the similarity of bond lengths of S1–P1 (1.9851(18) Å) and S2–P1 (1.975(2) Å) for **3**, S1–C33 (1.690(2) Å), S2–C33 (1.706(2) Å), S3–C70 (1.703(19) Å) and S4–C70 (1.711(18) Å) for **4**, indicate that the −1 charge of the dithioate is delocalized over both sulfur atoms. Different from complexes **2** and **3**, **4** has two independent molecules in one unit, which is similar to the reported complex [22].

3.4. Electrochemical properties

The electrochemical behaviors of the four complexes were examined by using cyclic voltammetry. The cathodic and anodic scans were carried out in THF and CH_2Cl_2 solution at 293 K, respectively. The redox potentials, measured relative to an internal ferrocenium/ferrocene reference (Fc^+/Fc), are listed in Table 4. On the basis of the onset potentials of the oxidation and reduction, the estimated HOMO and LUMO energy levels of these Ir complexes with regard to the energy level of ferrocene (4.80 eV below vacuum) are also listed in Table 4.

The electrochemistry of cyclometalated Ir(III) complexes has been thoroughly investigated. Reduction is generally considered to mainly occurs on the heterocyclic portion of the cyclometalated C^N ligands, whereas oxidation process largely involves the Ir–aryl center [23]. The complex **1** shows three reversible reduction waves consistent with the reduction of three C^N ligands of the complex. The other three complexes (**2**, **3** and **4**) undergo two reversible reduction processes with potentials ranging from −2.43 to −2.67 V, corresponding to the reduction of two C^N ligands of the complexes. These are in accordance with reported *tris*-cyclometalated and *bis*-cyclometalated iridium complexes, respectively [8,20,24]. Since all species have the same cyclometalating ligand, the LUMO of these complexes should be little affected by the nature of the ancillary LX ligands. In fact, under the current experimental conditions, the first and second reduction potentials of the complexes stay in a narrow range of −2.43 to −2.52 V and −2.64 to −2.67 V, respectively,

On the other hand, each of four complexes only displays a reversible one-electron oxidation process with the oxidative potential spanning a wide range from 0.51 to 0.72 V. Thompson et al. have systematically investigated the influence of ancillary ligands on HOMO energy of *bis*-cyclometalated iridium complexes and found that the ancillary ligands with stronger ligand field strength stabilize the HOMO [9]. Consistent with this, the dithiolate ligands with stronger ligand field strength than acetylacetone result in higher oxidation potentials and lower HOMO energy levels of complexes than acetylacetone.

Table 2
Crystal data and structure refinement for complexes **2**–**4**

Crystal data	**2** · CH_2Cl_2	**3**	**4**
Empirical formula	$C_{38}H_{35}O_4N_4Cl_2Ir$	$C_{36}H_{36}O_4N_4PS_2Ir$	$C_{74}H_{72}O_5N_{10}S_4Ir_2$
Formula weight	874.80	875.98	1694.06
Crystal system	Triclinic	Triclinic	Triclinic
Space group	$P\bar{1}$	$P\bar{1}$	$P\bar{1}$
a (Å)	10.2710(8)	11.943(2)	13.2095(18)
b (Å)	13.3034(10)	11.978(2)	16.274(2)
c (Å)	14.1672(11)	13.793(3)	19.153(3)
α (°)	92.3960(10)	70.35(3)	96.262(2)
β (°)	108.3660(10)	75.84(3)	99.371(2)
γ (°)	98.2710(10)	89.60(3)	102.316(2)
Volume (Å^3)	1810.2(2)	1795.6(6)	3924.4(9)
Z	2	2	2
Calculated density (Mg/m^3)	1.605	1.620	1.434
Absorption coefficient (mm^{-1})	3.881	3.923	3.546
Temperature (K)	293(2)	293(2)	293(2)
Wavelength (Mo Kα) (Å)	0.71073	0.71073	0.71073
Crystal size (mm)	$0.25 \times 0.19 \times 0.12$	$0.12 \times 0.10 \times 0.08$	$0.30 \times 0.20 \times 0.08$
F(000)	868	872	1688
Reflections collected/unique [R_{int}]	11 845/8077 [0.0741]	8129/8129 [0.0000]	27 902/13 664 [0.0521]
Goodness-of-fit on F^2	1.119	1.095	1.190
Final R indices [$I > 2\sigma(I)$]			
R_1[a]	0.0392	0.0308	0.0887
wR_2[b]	0.0698	0.0752	0.2481
R indices (F^2)			
R_1	0.0479	0.0410	0.1037
wR_2	0.0716	0.0853	0.2555

[a] $R_1 = \sum[|F_o| - |F_c|]/\sum|F_o|$.
[b] $wR_2 = \{\sum[w(F_o^2 - F_c^2)]/\sum(wF_o^2)\}^{1/2}$.

Table 3
Selected bond lengths (Å) and angles (°) for complexes **2**–**4**

Complex ***2***					
Ir(1)–C(2)	1.986(5)	Ir(1)–C(25)	1.978(5)	Ir(1)–N(1)	2.031(3)
Ir(1)–N(3)	2.029(4)	Ir(1)–O(1)	2.116(3)	Ir(1)–O(2)	2.120(4)
C(17)–O(1)	1.261(6)	C(19)–O(2)	1.280(6)		
C(25)–Ir(1)–C(2)	92.06(19)	C(25)–Ir(1)–N(3)	79.92(17)	C(2)–Ir(1)–N(3)	91.40(16)
C(25)–Ir(1)–N(1)	93.47(16)	C(2)–Ir(1)–N(1)	79.96(17)	N(3)–Ir(1)–O(1)	98.51(14)
O(1)–Ir(1)–O(2)	89.06(14)	N(3)–Ir(1)–N(1)	168.97(15)		
Complex ***3***					
Ir(1)–C(2)	2.032(4)	Ir(1)–C(18)	2.029(4)	Ir(1)–N(1)	2.015(3)
Ir(1)–N(3)	2.028(3)	Ir(1)–S(1)	2.5076(16)	Ir(1)–S(2)	2.4809(13)
P(1)–S(1)	1.9851(18)	P(1)–S(2)	1.975(2)		
N(1)–Ir(1)–C(18)	92.7(3)	N(1)–Ir(1)–C(2)	79. 4(3)	C(18)–Ir(1)–N(3)	78. 8(3)
C(2)–Ir(1)–N(3)	93. 3(3)	C(18)–Ir(1)–S(1)	95. 49(18)	C(2)–Ir(1)–S(1)	173. 4(2)
S(2)–Ir(1)– S(1)	79.66(6)	N(1)–Ir(1)–N(3)	168.32(13)		
Complex ***4***					
Ir(1)–C(12)	2.050(16)	Ir(1)–C(28)	2.052(16)	Ir(2)–C(64)	2.048(17)
Ir(2)–C(49)	2.052(19)	Ir(1)–N(2)	2.030(14)	Ir(1)–N(3)	2.038(14)
Ir(2)–N(7)	2.012(13)	Ir(2)–N(9)	2.034(13)	Ir(1)–S(1)	2.453(5)
Ir(1)–S(2)	2.438(5)	Ir(2)–S(3)	2.452(4)	Ir(2)–S(4)	2.446(5)
S(1)–C(33)	1.690(2)	S(2)–C(33)	1.706(2)	S(3)–C(70)	1.703(19)
S(4)–C(70)	1.711(18)				
N(2)–Ir(1)–C(12)	79.7(6)	N(2)–Ir(1)–C(28)	93.9(6)	N(3)–Ir(1)–C(28)	78.3(6)
C(12)–Ir(1)–C(28)	90.1(7)	N(2)–Ir(1)–S(2)	93.6(4)	C(12)–Ir(1)–S(2)	168.8(4)
S(2)–Ir(1)–S(1)	72.17(16)	N(2)–Ir(1)–N(3)	168.5(5)	C(64)–Ir(2)–S(3)	170.1(5)
N(7)–Ir(2)–C(64)	92.4(6)	N(7)–Ir(2)–C(49)	79.4(6)	N(7)–Ir(2)–S(4)	95.6(4)
N(7)–Ir(2)–S(3)	93.3(4)	N(7)–Ir(2)–N(9)	168.9(6)	S(4)–Ir(2)–S(3)	71.54(15)

Table 4
Electrochemical properties of the Ir complexes

Complex	$E^{ox}_{1/2}$ (V)[a,c]	$E^{red}_{1/2}$ (V)[b,c]	E^{ox}_{onset} (V)	E^{red}_{onset} (V)	HOMO (eV)[d]	LUMO (eV)[e]	ΔE (V)[c]
1	0.51	−2.66, −2.52, −2.44	0.24	−2.25	−5.04	−2.55	2.49
2	0.58	−2.65, −2.50	0.25	−2.26	−5.05	−2.54	2.51
3	0.72	−2.64, −2.43	0.45	−2.28	−5.25	−2.52	2.73
4	0.64	−2.67, −2.48	0.42	−2.27	−5.22	−2.53	2.69

[a] The oxidation potential was measured in CH_2Cl_2 solution at a concentration of 10^{-3} M and scan rate was 50 mV s^{-1}.
[b] The reduction potential was measured in THF solution at a concentration of 10^{-3} M and scan rate was 50 mV s^{-1}.
[c] Potential values are reported vs. Fc^+/Fc.
[d] Determined from the onset oxidation potential.
[e] Determined from the onset reduction potential.

3.5. Photophysical properties

Fig. 6 shows the absorption spectra of four complexes. Absorption peak wavelengths and the molar extinction coefficients are given in Table 5. Intense absorptions are observed in the ultraviolet region of the spectra, between 250 and 350 nm, which can be easily assigned to the spin-allowed π–π* transitions from cyclometalated ĈN ligands. Relatively weaker absorption bands in the range of 350–400 nm (inset of Fig. 6) are well resolved, ascribing to a spin-allowed metal-to-ligand charge transfer (^{1}MLCT) transition. The long tail extended to lower energies (in the range of 400–500 nm) can be likely associated with both ^{3}MLCT and ^{3}π–π* transitions, which gains considerable intensity by mixing with the ^{1}MLCT transition through the spin–orbit coupling [9,18,25].

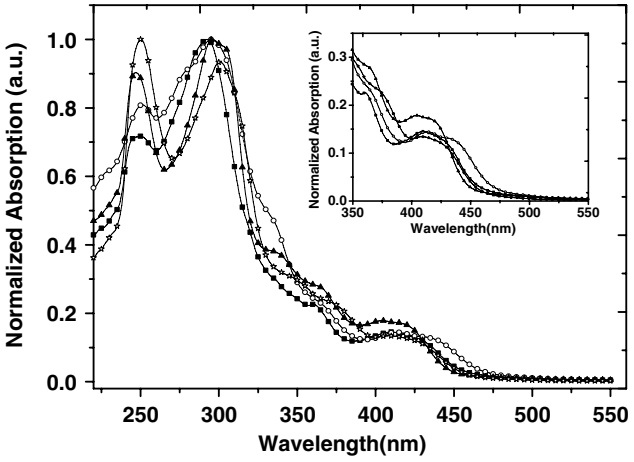

Fig. 6. Absorption spectra of complexes in CH_2Cl_2 solution at 298 K. (Inset: absorption bands in the range of 350–550 nm.)

Table 5
Photophysical data for $(tox)_2Ir(L\hat{}X)$ complexes

Complex	UV–Vis[a]	PL λ_{max} (nm)		Φ_f[c] (%)
	λ_{abs} (logε) (nm)	Solution[a]	Film[b]	
tox	274(4.0)	353	355	
1	246(3.8), 291(4.0), 361(3.4), 418(3.2), 456 (2.8)	520 548	522 550	28.3
2	251(3.9), 296(4.0), 367(3.3), 422(3.1), 454(2.8)	518 545	519 548	32.6
3	248(3.9), 296(4.0), 365(3.4), 410(3.2), 443(2.7)	501 536	506 542	13.2
4	250(4.0), 300(3.9), 373(3.4), 412(3.1), 445(2.7)	507 538	511 544	19.5

[a] In CH_2Cl_2 solution at 298 K.
[b] In PMMA film (7% weight ratio).
[c] Quantum yield was measured in CH_2Cl_2 solution relative to quinine bisulfate (10^{-5} M in 1.0 NH_2SO_4).

All complexes show strong luminescence both in solid state and in organic solutions upon irradiation by UV-light at ambient temperature. The PL spectra were measured in CH_2Cl_2 solution (Fig. 7) and in PMMA (polymethylmethacrylate) film (7% weight ratio) at 298 K, respectively. The vibronic fine structures in the PL spectra imply that the emissions predominantly result from ligand-centered $^3\pi$–π^* transition [2a,9,18]. The free ligand emits at 353 nm in CH_2Cl_2 solution. After coordinating with iridium, the maximum emitting wavelengths of the complexes were tuned to the range from 500 to 520 nm. Complex **1** with three cyclometalated ligands and **2** with β-diketonate ancillary ligand show almost same emitting spectra. Complexes **3** and **4** containing dithiolate ligand emit at maximum wavelengths of 501 and 507 nm, respectively, which falls in the blue to green region. A hypsochromic shift of 17 and 11 nm with respect to complex **2** took place. The altering of emission wavelength coincides with the varying of energy gap evaluated from the results of cyclic voltammetry. The complexes **2**–**4** have the almost equal LUMO energy level, whereas their HOMO level decrease with the ligand field strength of the ancillary ligands, and therefore the energy gap increases (vide supra).

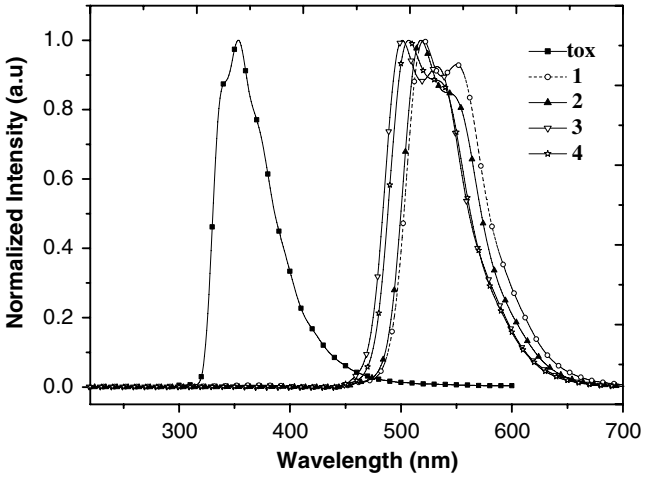

Fig. 7. PL spectra of complexes and free ligand in CH_2Cl_2 solution at 298 K.

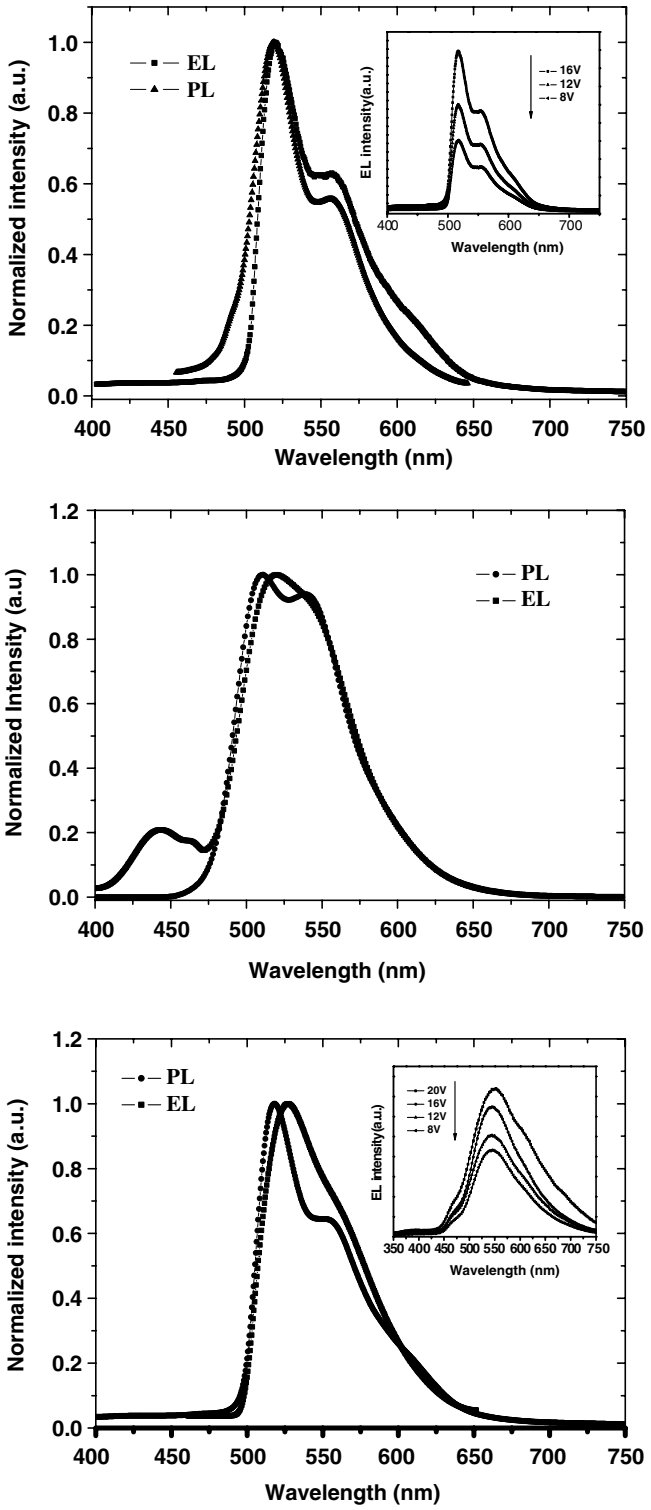

Fig. 8. EL spectra of devices using complex **2** (up), **3** (middle), **4** (bottom) as dopant, along with the corresponding PL spectrum in PMMA film for comparison. (Inset: EL spectra dependence on the driving voltage.)

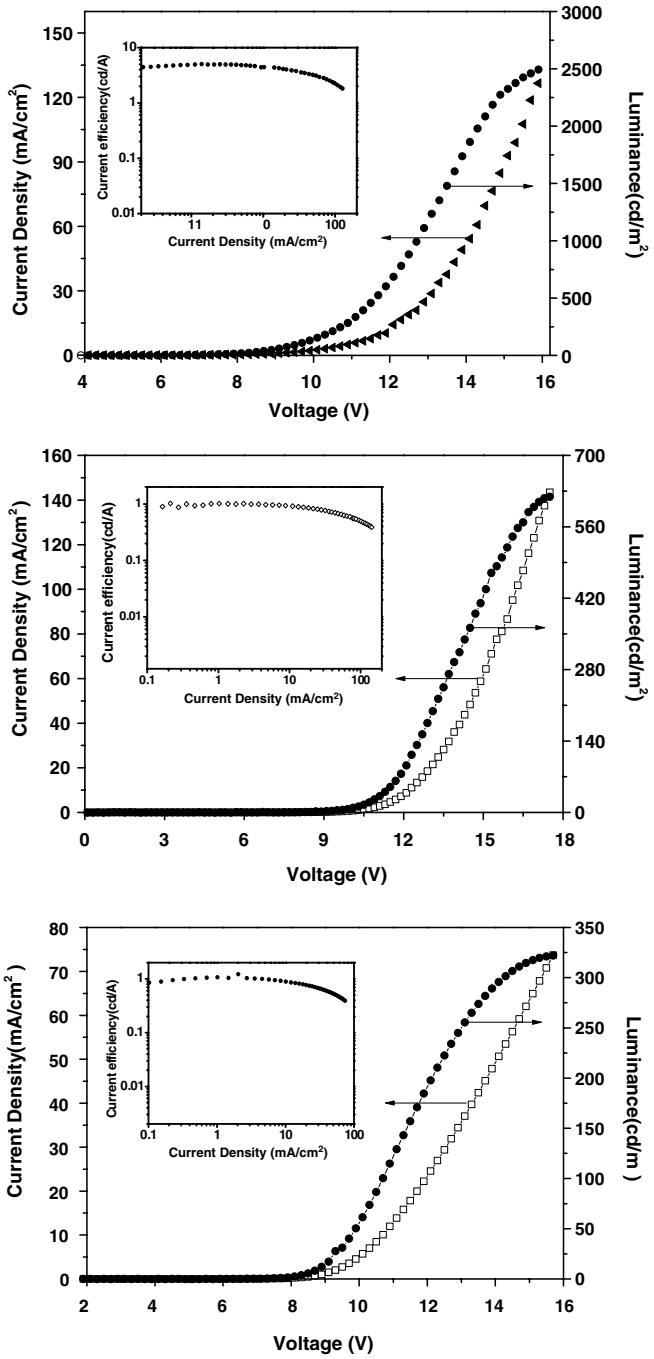

Fig. 9. Current density–voltage–brightness (*J*–*V*–*B*) of and dependence of current efficiency on current density (η_c–*J*) curve (inset) of the devices using complex **2** (up), **3** (middle), **4** (bottom) as dopant.

3.6. Electroluminescent properties

To understand the electroluminescent properties of these complexes, electroluminescent (EL) devices using complex **2**, **3** and **4** as dopant in the emitting layer have been fabricated, respectively. The EL device consists of multilayer films with the configuration of ITO/NPB (40 nm)/CBP + 7% dopant (30 nm)/BCP (10 nm)/AlQ_3 (30 nm)/LiF(1 nm)/Al (100 nm) [26]. Complex **2**, **3** and **4** were doped into the CBP as emissive layer at a concentration of 7%, which was in accordance with the doping concentration of the complex in PMMA film in photoluminescence. The EL spectra show that all the devices emit green light, with an emission peak very close in appearance to the photoluminescence spectra of the complexes in PMMA film, respectively, indicating that the EL emission of the device originates from the triplet excited states of the phosphors. The EL emission intensity shows a systematic decrease with decreasing driving voltage, but the EL emission peak is independent of the driving voltage (inset of Fig. 8).

Table 6
EL performances

Dopant phosphor	**2**	**3**	**4**
L (cd/m²)[a]	1235	425	156
L_{max} (cd/m²)	2592	635	339
η_c (cd/A)[a]	3.26	0.89	0.72
η_c (cd/A)[b]	2.23	0.64	0.52
$\eta_{c\,max}$ (cd/A)	5.28	1.08	1.24
J (mA/cm²)[c]	126	143	95
η_p (lm/W)[a]	2.56	1.62	0.96
η_p (lm/W)[b]	1.86	1.03	0.53
$\eta_{p\,max}$ (lm/W)	3.65	2.40	1.36
Voltage *V*[d]	15.2	17.5	13.8
V_{ON} *V*[e]	4.5	4.7	4.9
El_{max} (nm)	523	510	518

[a] Recorded at 20 mA/cm².
[b] Recorded at 100 A/cm².
[c] Current density at the maximum current efficiency.
[d] Voltage at the maximum brightness.
[e] Recorded at the brightness of 1 cd/m².

The current density–voltage–brightness (*J*–*V*–*B*) characteristics of the devices are shown in Fig. 9. The inset of Figure shows the current efficiency (η_c) as functions of current density (*J*) for the devices. Table 6 summarizes the performance of the devices. The device based on complex **2** shows good performance with a low turn-on voltage of 4.5 V and a maximum brightness of 2592 cd/m² at 15.2 V. A maximum current efficiency of 5.28 cd/A was obtained at a current density of 1.37 mA/cm². The device showed a gradual decreasing in η_c with increasing current density, but still remaining high η_c of 2.23 cd/A at the high current density of 100 mA/cm². This is attributed to increasing triplet–triplet annihilation of the phosphor-bound excitons. The device based on complex **3** shows the maximum current efficiency of 1.08 cd/A at the current density of 5.10 mA/cm² and the maximum brightness of 635 cd/m² at 17.5 V, whereas those for device based on complex **4** are 1.24 cd/A at 7.43 mA/cm² and 339 cd/m² at 13.8 V, respectively. It is obvious that the device using complex **2** with acac ancillary ligand as phosphorescent dopant exhibit better performance than that using complex **3**, **4** with dithiolate ancillary ligand.

4. Conclusions

In summary, the four iridium(III) complexes with 1,3,4-oxadiazole derivative as cyclometalated ligand for the first

time were synthesized. The solution structures of the complexes were established by using NMR spectra. The crystal structures of three complexes were determined by X-ray crystallography. To each complex, the Ir center locates at a distorted octahedral environment by the three chelating ligands with *trans*-N–N and *cis*-C–C dispositions. The electrochemistry results indicate the LOMO energy levels of the complexes are little disturbed by variation of the ancillary ligand, whereas the HOMO energy levels can be tuned by interaction of ancillary ligands with iridium d-orbitals. The stronger ligand field strength of the dithiolate ancillary ligands leads to lower HOMO energy levels of complexes than acetylacetone. Correspondingly, the energy gap of the complexes increases when dithiolate ancillary ligands replace acetylacetone, which is correlated with the hypsochromic shift of the emitting wavelength of complexes. The complexes containing dithiolate ligands emit at the wavelength of ca. 500 nm, which is in the blue to green region. This provides a route to prepare iridium phosphorescent materials in the blue to green, even blue emission region. The electroluminescent properties of the complexes were investigated. All devices have a low turn-on voltage in the range of 4.5 and 4.9 V. A high-efficiency green emission has been demonstrated in device using complex **2** with acetylacetone ancillary ligand as doping emitter.

5. Supplementary material

Crystallographic data for the structural analyses have been deposited with the Cambridge Crystallographic Data Center, CCDC reference numbers for **2**·CH_2Cl_2, **3** and **4** are 293690, 293691 and 293692, respectively. Copies of this information may be obtained free of charge from The Director, CCDC, 12 Union Road, Cambridge, CB2 1EZ UK (fax: +44 1223 336033; email: deposit@ccdc.cam.ac.uk or www: http://www.ccdc.cam.ac.uk).

Acknowledgements

We thank the National Natural Science Foundation of China (Project Nos. 20371036 and 20474047), the Program for New Century Excellent Talents in University, the Ministry of Education of China, the Hubei Province Science Fund for Distinguished Young Scholar (No. 2003ABB008) for financial support. We are grateful for valuable discussion with Professor M.L.H. Green, Oxford University, in the NMR spectra.

References

[1] (a) K. Kalyanasundaran, Coord. Chem. Rev. 46 (1982) 159;
(b) K. Kalyanasundaram, M. Gratzel, Coord. Chem. Rev. 177 (1998) 347;
(c) V. Balzani, F. Scandola, Supramolecular Photochemistry, Ellis Horwood, Chichester, UK, 1991;
(d) V. Balzani, A. Credi, F. Scandola, in: L. Fabbrizzi, A. Poggi (Eds.), Transition Metals in Supramolecular Chemistry, Kluwer, Dordrecht, The Netherlands, 1994, p. 1;
(e) J. Lehn, Supramolecular Chemistry Concepts and Properties, VCH, Weinheim, Germany, 1995;
(f) J.K. Lee, D. Yoo, M.F. Rubner, Chem. Mater. 9 (1997) 1710;
(g) F.G. Gao, A. Bard, J. Am. Chem. Soc. 122 (2000) 7426;
(h) K. Wang, L. Huang, L. Gao, L. Jin, C. Huang, Inorg. Chem. 41 (2002) 3353;
(i) N. Sonoyama, O. Karasawa, Y. Kaizu, J. Chem. Soc., Faraday Trans. 91 (1995) 437;
(j) Y. Ma, H. Zhang, J. Shen, C. Che, Synth. Met. 94 (1998) 245;
(k) Q. Liu, L. Thorne, I. Kozin, D. Song, C. Seward, M.D. Iorio, Y. Tao, S. Wang, J. Chem. Soc., Dalton Trans. (2002) 3234;
(l) Y. Kang, J. Lee, D. Song, S. Wang, Dalton Trans. (2003) 3493;
(m) B.W. Ma, J. Li, P.I. Djurovich, M. Yousufuddin, R. Bau, M.E. Thompson, J. Am. Chem. Soc. 127 (2005) 28;
(n) Y. Amao, Y. Ishikawa, I. Okura, Anal. Chim. Acta 445 (2001) 177;
(o) S.M. Zakeeruddin, D.M. Fraser, M.K. Nazeeruddin, M. Grätzel, J. Electroanal. Chem. 337 (1993) 2536.

[2] (a) S. Lamansky, P. Djurovich, D. Murphy, F. Abdel-Razzaq, R. Kwong, I. Tsyba, M. Bortz, B. Mui, R. Bau, M.E. Thompson, Inorg. Chem. 40 (2001) 1704;
(b) M.K. Nazeeruddin, R. Humphry-Baker, D. Berner, S. Rivier, L. Zuppiroli, M. Graetzel, J. Am. Chem. Soc. 125 (2003) 8790;
(c) J. Kim, I.S. Shin, H. Kim, J.K. Lee, J. Am. Chem. Soc. 127 (2005) 1614;
(d) W. Zhu, Y. Mo, M. Yuan, W. Yang, Y. Cao, Appl. Phys. Lett. 80 (2002) 2045;
(e) C.H. Yang, C. Tai, I. Sun, J. Mater. Chem. 14 (2004) 947;
(f) P.T. Furuta, L.S. Deng, M.E. Thompson, J.M. Frechet, J. Am. Chem. Soc. 126 (2004) 15388;
(g) Z.L. Shen, P.E. Burrows, V. Bulorvic, S.R. Forrest, M.E. Thompson, Science 276 (1997) 2009;
(h) J. Brooks, Y. Babayan, S. Lamansky, P.I. Djurovich, I. Tsyba, R. Bau, M.E. Thompson, Inorg. Chem. 41 (2002) 3055;
(i) J. Duan, P. Sun, C. Cheng, Adv. Mater. 15 (2003) 224.

[3] (a) W. Chien, A.T. Hu, J. Duan, D.K. Raybarapu, C. Chien, J. Organomet. Chem. 689 (2004) 4882;
(b) W. Huang, J. Lin, C. Chien, Y. Tao, S. Sun, Y. Wen, Chem. Mater. 16 (2004) 2480;
(c) S. Lamansky, P. Djurovich, D. Murphy, F. Abdel-Razzaq, H.F. Lee, C. Adachi, P.E. Burrows, S.R. Forrest, M.E. Thompson, J. Am. Chem. Soc. 123 (2001) 4304.

[4] (a) H. Gregory, R.B. Martin, J. Mater. Chem. 15 (2005) 94;
(b) H. Tokuhisa, M. Era, T. Tsutsui, Appl. Phys. Lett. 72 (1998) 2639;
(c) M. Strukelj, F. Papadimitrakopoulos, T.M. Miller, L.J. Rothberg, Science 265 (1995) 1969.

[5] (a) H. Denis, T. Dimitris, Chem. Mater. 15 (2003) 2079;
(b) Z. Peng, J.H. Zhang, Chem. Mater. 11 (1999) 1138;
(c) Z. Bao, Z. Peng, M.E. Galvin, E.A. Chandross, Chem. Mater. 10 (1998) 1201;
(d) Z. Peng, Z. Bao, M.E. Galvin, Adv. Mater. 10 (1998) 680;
(e) Z. Peng, Z. Bao, M.E. Galvin, Chem. Mater. 10 (1998) 2086;
(f) N.C. Greenham, S.C. Moratti, D.D.C. Bradley, R.H. Friend, A.B. Holmes, Nature 365 (1993) 628;
(g) S.C. Moratti, R. Cervimi, A.B. Holmes, D.R. Baigent, R.H. Friend, N.C. Greenham, J. Gruner, P.J. Hamer, Synth. Met. 17 (1995) 2117;
(h) J.S. Yang, T.M. Swager, J. Am. Chem. Soc. 120 (1998) 5321;
(i) Q. Pei, Y. Yang, Chem. Mater. 7 (1995) 1568;
(j) W. Huang, W.L. Yu, H. Meng, J. Pei, S.F. Li, Chem. Mater. 10 (1998) 3340;
(k) J.P. Lu, R.H. Antisar, Y. Sun, S.H. Allan, M. Tony, J.P. Dodelet, Chem. Mater. 11 (1999) 2501;
(l) E. Buchwald, M. Meier, S. Karg, P. Pösch, H.W. Schmidt, P. Strohriegl, W. Riess, M. Schwoerer, Adv. Mater. 7 (1995) 839;
(m) F. Cacialli, X. Li, R.H. Friend, S.C. Moratti, A.B. Holmes, Synth. Met. 75 (1995) 161;

(n) X.C. Li, F. Cacialli, M. Gilles, J. Gruner, R.H. Friend, A.B. Holmes, S.C. Moratti, T.M. Yong, Adv. Mater. 7 (1995) 898;
(o) N. Tamoto, C. Adachi, K. Nagai, Chem. Mater. 9 (1997) 1077.
[6] (a) Y. Hamada, T. Sano, K. Shibata, K. Kuroki, Jpn. J. Appl. Phys., Part 2 34 (1995) L824;
(b) J. Kido, H. Shionoya, K. Nagai, Appl. Phys. Lett. 67 (1995) 2281;
(c) C.C. Wu, J.C. Sturm, R.A. Register, J. Tian, E.P. Dana, M.E. Thompson, IEEE Trans. Electron Dev. 44 (1997) 1269;
(d) C.C. Wu, J.C. Sturm, R.A. Register, M.E. Thompson, Appl. Phys. Lett. 69 (1996) 3117;
(e) A.R. Brown, D.D.C. Bradley, J.H. Burroughes, R.H. Friend, N.C. Greenham, Appl. Phys. Lett. 61 (1992) 2793;
(f) C. Adachi, S. Tokito, T. Tsutsui, S. Saito, Jpn. J. Appl. Phys. 27 (1988) L713;
(g) W. Huang, H. Meng, W. Yu, J. Gao, A. Heeger, Adv. Mater. 10 (1998) 593;
(h) W. Yu, H. Meng, J. Pei, Y.H. Lai, S.J. Chua, W. Huang, Chem. Commun. 18 (1998) 1957;
(i) W. Yu, H. Meng, J. Pei, W. Huang, J. Am. Chem. Soc. 120 (1998) 11808.
[7] F. Zamora, S. Rico, P. Amo-Ocboa, J. Inorg. Biochem. 68 (1997) 257.
[8] (a) F.W.M. Vanhelmont, H.U. Güdel, M. Förtsch, H. Bürgi, Inorg. Chem. 36 (1997) 5512;
(b) W.J. Finkenzeller, H. Yersin, Chem. Phys. Lett. 377 (2003) 299;
(c) W.J. Finkenzeller, P. Stoessel, H. Yersin, Chem. Phys. Lett. 397 (2004) 289;
(d) H. Yersin, W. Humbs, Inorg. Chem. 38 (1999) 5820.
[9] J. Li, P.I. Djurovich, B.D. Alleyne, M. Yousufuddin, N.N. Ho, J.C. Thomas, J.C. Peters, R. Bau, M.E. Thompson, Inorg. Chem. 44 (2005) 1713.
[10] (a) G. Suardi, B.P. Cleary, S.B. Duckett, C. Sleigh, R. Melinda, E.W. Reed, R. Eisenberg, J. Am. Chem. Soc. 119 (1997) 7716;
(b) Y.A. Lee, J.E. Mcgarrah, R.J. Lachicotte, R. Eisenberg, J. Am. Chem. Soc. 124 (2002) 10662.
[11] (a) B.B. Xu, Y.C. Pan, J.H. Zhang, Z.H. Peng, Synth. Met. 114 (2000) 337;
(b) Y.M. Sun, C.S. Wang, Polymer 42 (2001) 1035.
[12] C.G. Krespan, J. Am. Chem. Soc. 83 (1961) 3434.
[13] R.W. Young, K.H. Wood, J. Am. Chem. Soc. 77 (1955) 400.
[14] G.M. Sheldrick, SHELX-97. Structure Solution and Refinement Package, Universität Göttingen, Göttingen, Germany, 1997.
[15] Program DIFABS for empirical absorption corrections: N. Walker, D. Stuart, Acta Crystallogr. A 39 (1983) 158.
[16] L.J. Farrugia, J. Appl. Crystallogr. 30 (1997) 565.
[17] M. Nonoyama, Bull. Chem. Soc. Jpn. 47 (1974) 767.
[18] A.B. Tamayo, B.D. Alleyne, P.I. Djurovich, S. Lamansky, I. Tsyba, N.N. Ho, R. Bau, M.E. Thompson, J. Am. Chem. Soc. 125 (2003) 7377.
[19] F.O. Garces, K.A. King, R.J. Watts, Inorg. Chem. 27 (1988) 3464.
[20] (a) K.A. King, P.J. Spellane, R.J. Watts, J. Am. Chem. Soc. 107 (1985) 1431;
(b) S. Sprouse, K.A. King, P.J. Spellane, R.J. Watts, J. Am. Chem. Soc. 106 (1984) 6647;
(c) K.A. King, R.J. Watts, J. Am. Chem. Soc. 109 (1987) 1589;
(d) Y. Ohsawa, P.J. Spellane, K.A. King, M.K. DeArmond, K.W. Hanck, R.J. Watts, J. Phys. chem. 91 (1987) 1047;
(e) M.G. Colombo, H.U. Güdel, Inorg. Chem. 32 (1993) 3081;
(f) M.G. Colombo, A. Hauser, H.U. Güdel, Inorg. Chem. 32 (1993) 3088;
(g) M.G. Colombo, T.C. Brunold, T. Riedener, H.U. Güdel, M. Förtsch, Hans-Beat Bürgi, Inorg. Chem. 33 (1994) 545.
[21] (a) F.O. Garces, K. Dedeian, N.L. Keger, R.J. Watts, Acta Crystallogr. C 49 (1993) 1117;
(b) I.R. Laskar, T. Chen, Chem. Mater. 16 (2004) 111.
[22] A.J. Sandee, C.K. Williams, N.R. Evans, J.E. Davies, C.E. Boothby, A. Köhler, R.H. Friend, A.B. Holmes, J. Am. Chem. Soc. 126 (2004) 7041.
[23] (a) J. Pommerehne, H. Vestweber, W. Guss, R.F. Mahrt, H. Bässler, M. Porsch, J. Daub, Adv. Mater. 7 (1995) 551;
(b) P.J. Hay, J. Phys. Chem. A 106 (2002) 1634.
[24] F. Wu, H. Su, C. Shu, L. Luo, W. Diau, C. Chien, J. Duan, G. Lee, J. Mater. Chem. 15 (2005) 1035.
[25] C. Adachi, M.A. Baldo, S.R. Forrest, M.E. Thompson, Appl. Phys. Lett. 781 (2000) 704.
[26] Q. Zhang, Q. Zhou, Y. Cheng, L. Wang, D. Ma, X. Jing, Adv. Mater. 16 (2004) 432.